Journal of Computational Physics 429 (2021) 109996

Contents lists available at ScienceDirect

Journal of Computational Physics

www.elsevier.com/locate/jcp

Efficient smoothed particle radiation hydrodynamics I: Thermal radiative transfer

Brody R. Bassett *, J. Michael Owen, Thomas A. Brunner

Lawrence Livermore National Laboratory, 7000 East Avenue, Livermore, CA, 94550, United States of America

ARTICLE INFO

Article history:
Received 7 January 2020
Received in revised form 27 October 2020
Accepted 6 November 2020
Available online 25 November 2020

Keywords:
Radiation hydrodynamics
Smoothed particle hydrodynamics
Radiative transfer
Meshless method

ABSTRACT

This work presents efficient solution techniques for radiative transfer in the smoothed particle hydrodynamics discretization. Two choices that impact efficiency are how the material and radiation energy are coupled, which determines the number of iterations needed to converge the emission source, and how the radiation diffusion equation is solved, which must be done in each iteration. The coupled material and radiation energy equations are solved using an inexact Newton iteration scheme based on nonlinear elimination, which reduces the number of Newton iterations needed to converge within each time step. During each Newton iteration, the radiation diffusion equation is solved using Krylov iterative methods with a multigrid preconditioner, which abstracts and optimizes much of the communication when running in parallel. The code is verified for an infinite medium problem, a one-dimensional Marshak wave, and a two and three-dimensional manufactured problem, and exhibits first-order convergence in time and second-order convergence in space. For these problems, the number of iterations needed to converge the inexact Newton scheme and the diffusion equation is independent of the number of spatial points and the number of processors.

© 2020 Elsevier Inc. All rights reserved.

1. Introduction

Smoothed particle hydrodynamics (SPH) is a meshless approach to solving the hydrodynamics equations, in which the fluid is separated into discrete masses that are used as interpolation points (for an overview, see Refs. [1,2]). SPH has several desirable properties, such as automatic conservation of mass and enforced conservation of energy and momentum, flexible point topology, and Galilean invariance. Like mesh-based Lagrangian codes, the resolution of the problem follows the mass, but unlike mesh-based codes, SPH does not have issues with mesh tangling. Drawbacks of SPH include a lack of zeroth-order consistency (the interpolant cannot generally reproduce a constant exactly) [3] and additional expense that comes from computing connectivity at each time step. There are extensions to SPH that correct some of these issues, such as moving least squares particle hydrodynamics [4,5] and conservative reproducing kernel smoothed particle hydrodynamics [6].

The thermal radiative transfer equations have been solved using a smoothed particle hydrodynamics discretization previously. The most popular method is implicit, two-temperature, flux-limited diffusion, first implemented in Refs. [7,8]. These papers assume an ideal gas equation of state. In the latter paper, the system is reduced to solving a quartic equation per point within a Gauss-Seidel iteration scheme. This method has been extended to include the physics of a diffuse interstellar

* Corresponding author.
E-mail addresses: bassett4@llnl.gov (B.R. Bassett), owen8@llnl.gov (J.M. Owen), brunner6@llnl.gov (T.A. Brunner).

https://doi.org/10.1016/j.jcp.2020.109996
0021-9991/© 2020 Elsevier Inc. All rights reserved.

medium for star formation [9]. There are other implementations of flux-limited diffusion, most of which have been applied to astrophysical problems [10,11]. The form of the second derivative used most often for the radiation diffusion second derivative was first applied to heat diffusion [12]. The optically-thin variable Eddington factor equations with Eddington factors determined by source information (as opposed to by a full transport calculation) have been applied to cosmological simulation [13]. Similar methods that have been studied include ray-tracing [14], Monte Carlo [15], and neutrino flux-limited diffusion [16].

Thermal radiative transfer couples the transport of photons with the hydrodynamic state. Common coupling techniques for the radiation and material equations include simple convergence of the residuals of both equations (including Newton-Krylov methods), using a single Newton iteration, lagging the nonlinear terms in the equation, predictor-corrector schemes, and linearization of the nonlinear emission source [17,18]. Another common method is linear multifrequency-grey acceleration, which accelerates multigroup convergence and can be used as a preconditioner for a Krylov iterative solve [19,20]. For more information on time discretization methods, see the following papers, which compare time integration methods for radiative transfer: block Jacobi, Schur complement, and operator splitting approaches [21]; Newton's method, Newton-Krylov, and linearized approaches [17]; and Newton's method, linearized approaches, and operator splitting [22]. A common thread among these is that while full Newton's method is expensive, it is more stable than the alternatives. The method used in this paper is based on nonlinear elimination methods, as described in Ref. [23] and applied to radiation diffusion in Ref. [24], which fully converges the nonlinear solution with only a marginal cost increase over the linearized solution.

The radiation diffusion and transport equations have also been solved using meshless methods other than SPH, including for coupled radiative transport and conductive heat transfer [25–27], neutron transport [28], and neutron diffusion [29,30]. Many of these discretizations involve either relatively flat meshless functions (which increases accuracy but makes the system ill-conditioned) or integration of the meshless functions. The advantage of using the SPH discretization directly is that the same functions that are used for hydrodynamics can be reused for the radiation, without recomputing the topology.

Some particle methods map unknowns to a background grid for certain physics, such as electromagnetic particle-in-cell methods that map the charge of the particles to a background grid for the solution of Maxwell's equations [31]. A similar method could be employed for radiation diffusion with SPH, in which the density and material energy would be mapped to a background mesh for a radiation diffusion solve, but this would introduce complications with mesh creation and diffusivity due to the mapping. For consistent SPH diffusion, the solution points are the same for hydrodynamics and radiation, which simplifies the solution process and eliminates possible errors due to mapping. SPH diffusion is not computationally competitive with mesh-based diffusion due to the large number of neighbors, but is compatible with SPH hydrodynamics, which can handle problems that mesh-based methods struggle with.

The goal of this research is to make SPH radiation diffusion more efficient. This is done by improving the solution of the diffusion problem using fast and accurate preconditioners and applying material-radiation coupling methods that speed up the convergence of the radiation emission and absorption. With appropriate time step constraints, the solver is stable and exhibits first-order convergence in time and second-order convergence in space to analytic solutions and manufactured problems. The methods used here scale well with the number of points and under domain decomposition due to the use of fast multigrid solvers [32], which also makes the method simple to implement on distributed architectures. The remainder of this paper is structured as follows. In Sec. 2, the SPH thermal radiative transfer equations are derived and discretized in time and space. In Sec. 3, the implementation of the equations is discussed. Finally, in Sec. 4, results for problems in one, two and three dimensions with known solutions are presented to verify the accuracy of the code. In Paper II, the full SPH radiation hydrodynamics equations are derived with appropriate radiation-material coupling terms, and results for full radiation hydrodynamics are presented.

2. Theory

The smoothed particle hydrodynamics method is used to discretize the thermal radiative transfer equations in space. The discretization in time reduces a coupled set of equations for the material and radiation energies to separate updates for the material and radiation energies in an iterative process. The resulting equations conserve energy.

2.1. The thermal radiative transfer equations

The thermal radiative transfer equations are

$$\rho \partial_t e = -c\sigma_a B + c\sigma_a E + Q_e, \tag{1a}$$

$$\partial_t E = -\partial_x^\alpha F^\alpha - c\sigma_a E + c\sigma_a B + Q_E, \tag{1b}$$

$$\frac{1}{c}\partial_t F^\alpha = -c\partial_x^\beta P^{\alpha\beta} - \sigma_t F^\alpha, \tag{1c}$$

with the variables

t, time,
x, position,

ρ, mass density,
e specific material energy,
E, radiation energy density,
F^{α}, radiation flux,
$P^{\alpha\beta}$, radiation pressure,
T, material temperature,
B, integrated photon emission function,
c, speed of light in a vacuum,
σ_t, total opacity,
σ_a, absorption opacity,
a, black-body constant,
Q_e, nonhomogeneous material energy source,
Q_E, nonhomogeneous radiation energy source.

Greek letters used as superscripts (e.g. F^{α}) indicate dimensional components of a vector. For derivatives, a similar definition holds, where $\partial_x^{\alpha} E$ would indicate the α component of the gradient of E with respect to x. Repeated indices indicate summation, so $\partial_x^{\alpha} F^{\alpha}$ is the divergence of F with respect to x.

The radiation transport equation has been integrated over all energy frequencies (the grey approximation) and integrated over angle to produce the first two angular moments. For the derivation in Paper I, the material is assumed to be stationary. The emission term is defined as

$$B = aT^4, \tag{2}$$

where the black body constant a is defined in terms of the Stefan-Boltzmann constant σ_{SB} and the speed of light c as $a = 4\sigma_{SB}/c$. The material energy and temperature are connected through an equation of state. An example is the ideal gas equation of state, in which the temperature is proportional to the energy,

$$T = \frac{\mu\,(\gamma - 1)\, m_p}{k_B} e, \tag{3}$$

where μ is the molecular mass, k_B is the Boltzmann constant, and γ is the ratio of heat capacities. The opacities generally depend on material, temperature and density.

Assuming the specific intensity is linearly anisotropic in angle, the pressure term becomes

$$P^{\alpha\beta} = \frac{1}{3} I_{\alpha\beta} E, \tag{4}$$

where I is the tensor identity. Assuming that the time derivatives are neglected, the first angular moment of the transport equation [Eq. (1b)] can be solved for the radiation flux to get Fick's law,

$$F^{\alpha} = -\frac{c}{3\sigma_t} \partial_x^{\alpha} E. \tag{5}$$

Replacing the flux term in the zeroth angular moment equation [Eq. (1c)] with Fick's law and replacing the pressure term by the linearly anisotropic value results in the diffusion equation,

$$\partial_t E = \partial_x^{\alpha} \frac{c}{3\sigma_t} \partial_x^{\alpha} E - c\sigma_a E + c\sigma_a B + Q_E. \tag{6}$$

In the original radiation equations [Eqs. (1b) and (1c)], if the pressure were not isotropic, the radiation would propagate correctly at the speed of light. However, when the time derivative on the first moment equation is dropped, this adds an error that allows the radiation to propagate faster than the speed of light, $|\boldsymbol{F}| > cE$. This effect can be prevented by applying a flux limiter λ to the diffusion equation,

$$\partial_t E = \partial_x^{\alpha} \frac{c\lambda}{\sigma_t} \partial_x^{\alpha} E - c\sigma_a E + c\sigma_a B + Q_E. \tag{7}$$

With a constant $\lambda = 1/3$, the original equation is recovered. The flux limiter is usually written in terms of the constant R,

$$R = \frac{\sqrt{\left(\partial_x^{\alpha} E\right)\left(\partial_x^{\alpha} E\right)}}{\sigma_t E}, \tag{8}$$

with examples such as the Levermore flux limiter [33],

$$\lambda = \frac{2 + R}{6 + 3R + R^2}, \tag{9}$$

and the Larsen flux limiter [34],

$$\lambda = \frac{1}{\left(3^k + R^k\right)^{1/k}}, \tag{10}$$

where k is a chosen constant. Both of these have the correct limits for diffusive regions ($R \to 0$), which is the diffusion equation, and optically thin regions ($R \to \infty$), which describes radiation propagating at the speed of light [35],

$$F^\alpha \to \begin{cases} -\frac{c}{3\sigma_t}\partial_x^\alpha E, & R \to 0, \\ -\frac{\partial_x^\alpha E}{\sqrt{\left(\partial_x^\beta E\right)\left(\partial_x^\beta E\right)}} cE, & R \to \infty. \end{cases} \tag{11}$$

The Larsen flux limiter with $k = 2$ is used in most of the results in this paper.

2.2. Time discretization

The coupled material and radiation energy equations [Eqs. (1a) and (7)] are discretized fully implicitly in time, using the nonlinear elimination methodology described in Ref. [24]. The derivation begins with the coupled material and radiation diffusion equations discretized using backward Euler,

$$\boldsymbol{G} = \begin{bmatrix} m\left(e^n, E^n\right) \\ r\left(e^n, E^n\right) \end{bmatrix} = \begin{bmatrix} \frac{\rho}{\Delta t}\left(e^n - e^{n-1}\right) + c\sigma_a B^n - c\sigma_a E^n - Q_e^n \\ \frac{1}{\Delta t}\left(E^n - E^{n-1}\right) - \partial_x^\alpha \frac{c\lambda}{\sigma_t}\partial_x^\alpha E^n + c\sigma_a E^n - c\sigma_a B^n - Q_E^n \end{bmatrix} = \begin{bmatrix} 0 \\ 0 \end{bmatrix}, \tag{12}$$

where $\boldsymbol{U} = \begin{bmatrix} e & E \end{bmatrix}^\top$. Newton's method updates the state according to

$$\boldsymbol{J}^\ell \boldsymbol{\delta}^\ell = -\boldsymbol{G}^\ell, \tag{13a}$$

$$\boldsymbol{U}^{\ell+1} = \boldsymbol{U}^\ell + \boldsymbol{\delta}^\ell, \tag{13b}$$

where $\boldsymbol{J}$ is the Jacobian with respect to e and E,

$$\boldsymbol{J} = \begin{bmatrix} J_{m,e} & J_{m,E} \\ J_{r,e} & J_{r,E} \end{bmatrix} = \begin{bmatrix} \frac{\rho}{\Delta t} + \frac{c}{c_v}\sigma_a \partial_T B & -c\sigma_a \\ -\frac{c}{c_v}\sigma_a \partial_T B & \frac{1}{\Delta t} - \partial_x^\alpha \frac{c\lambda}{\sigma_t}\partial_x^\alpha + c\sigma_a \end{bmatrix}, \tag{13c}$$

and $\boldsymbol{\delta} = [\delta_e, \delta_E]^\top$ is the change in the state variables and $c_v = \frac{\partial e}{\partial T}$ is the specific heat capacity.

To simplify the Newton iteration, the Schur compliment of the Jacobian is taken, resulting in the Jacobian system

$$\begin{bmatrix} J_{m,e} & J_{m,E} \\ 0 & J_{r,E} - J_{r,e}J_{m,e}^{-1}J_{m,E} \end{bmatrix} \begin{bmatrix} \delta_e \\ \delta_E \end{bmatrix} = \begin{bmatrix} -G_m \\ -G_r + J_{r,e}J_{m,e}^{-1}G_m \end{bmatrix} \tag{14}$$

that can be solved first for δ_E and then δ_e. This system of equations can be first solved for δ_E and then δ_e. The solution in Eq. (14) combined with the update in Eq. (13b) is full Newton iteration without approximation. Noting that $\partial_T B = 4aT^3$, the term $J_{r,e}J_{m,e}^{-1}$ can be written in terms of the Fleck factor commonly used in implicit Monte Carlo [36],

$$f = \left(1 + c\sigma_a \Delta t \frac{4aT^3}{\rho c_v}\right)^{-1}, \tag{15}$$

which is used to forward-predict the emission source, as

$$J_{r,e}J_{e,e}^{-1} = f - 1. \tag{16}$$

Finally, the temperature is held constant in f during each time step, which results in an inexact Newton iteration scheme,

$$\frac{1}{\Delta t}E^{n,\ell+1} - \partial_x^\alpha \frac{c\lambda}{\sigma_t}\partial_x^\alpha E^{n,\ell+1} + c\sigma_a f E^{n,\ell+1} = \frac{1}{\Delta t}E^{n-1} + c\sigma_a B^{n,\ell} - (1-f)c\sigma_a E^{n,\ell} + Q_E^n, \tag{17}$$

with the time step index n and the iteration index ℓ. When E^n has converged, the terms involving f in the diffusion equation cancel out and the original, time-discretized diffusion equation is recovered.

Equations (13) represent the standard Newton solution method for the thermal radiative transfer equations. Here, a nonlinear acceleration technique from Ref. [24] is additionally applied. The following two functions are helpful in describing the iterative process of solving the equations,

$$m\left(e^{\star}, E\right) = \frac{\rho}{\Delta t}\left(e^{\star} - e^{n-1}\right) + c\sigma_a B^{\star} - c\sigma_a E - Q_e^n = 0, \tag{18a}$$

$$r^{\dagger}\left(e, E, E^{\star}\right) = \frac{1}{\Delta t}E^{\star} - \partial_x^{\alpha}\frac{c\lambda}{\sigma_t}\partial_x^{\alpha}E^{\star} + c\sigma_a f E^{\star} - \frac{1}{\Delta t}E^{n-1} - c\sigma_a B + (1-f)\,c\sigma_a E - Q_E^n = 0 \tag{18b}$$

where $e^{\star}$ and $E^{\star}$ represent the values to be solved for. Note the use of $r^{\dagger}$ to distinguish the diffusion equation from the starting equation r. The solution of $r^{\dagger}(e, E, E^{\star}) = 0$ represents solving a spatially-coupled linear equation, as discussed in Sec. 3.2. Note that the value of the material energy in these equations is entirely dependent on the radiation energy, which means that a solution of $r^{\dagger}$ represents an inexact Newton iteration of the full material and radiation energy system. After a solution of $r^{\dagger}$ for the radiation energy, the material energy is updated by solving $m(e^{*}, E) = 0$, which represents a nonlinear solve using Newton's method,

$$e^{\star} \leftarrow e^{\star} - \left(J_{m,e}^{\star}\right)^{-1}\left[\frac{\rho}{\Delta t}\left(e^{\star} - e^{n-1}\right) + c\sigma_a B^{\star} - c\sigma_a E - Q_e^n\right], \tag{19}$$

where $\leftarrow$ represents an update to the value of $e^{\star}$. This update is performed until $e^{\star}$ is converged. This differs from standard Newton iteration, where the material energy update would be done simultaneously with the radiation energy update and without solving $m(e^{*}, E) = 0$ until e^{*} is converged. The iterative solution procedure for these two equations is described in Algorithm 1. Note that because the material energy has been eliminated through the nonlinear elimination process and can be considered a function of the radiation energy E, not an independent variable. This means that when the radiation energy is updated, the material energy is recomputed. The initial update makes the material energy consistent with the value of the radiation energy before iterations start.

Algorithm 1 Material and radiation energy update, which is based on Ref. [24]. The material and radiation energy equations m and $r^{\dagger}$ are defined in Eq. (18), while the Newton update for m is described in Eq. (19). The convergence criteria are defined in Eqs. (20).

```
ℓ = 0
set initial guesses to e^{n,ℓ} = e^{n-1} and E^{n,ℓ} = E^{n-1}
solve m(e^{n,ℓ}, E^{n,ℓ}) = 0 for e^{n,ℓ}
   (perform Newton updates until converged to inner tolerance for e)
while e^n and E^n not converged to outer tolerances do
   solve r†(e^{n,ℓ}, E^{n,ℓ}, E^{n,ℓ+1}) = 0 for E^{n,ℓ+1}
      (if iterative solver is used, iterate until converged to inner tolerance for E)
   solve m(e^{n,ℓ+1}, E^{n,ℓ+1}) = 0 for e^{n,ℓ+1}
      (perform Newton updates until converged to inner tolerance for e)
   ℓ = ℓ + 1
end while
```

The outer iterations, or the inexact Newton iteration of the material and radiation energy system, continue until the convergence criteria are met,

$$\left|\frac{e^{n,\ell+1} - e^{n,\ell}}{e^{n,\ell+1}}\right| < \epsilon_e, \tag{20a}$$

$$\left|\frac{E^{n,\ell+1} - E^{n,\ell}}{E^{n,\ell+1}}\right| < \epsilon_E. \tag{20b}$$

The inner iterations, or the iterations required to converge m and r within an outer iteration, use similar equations for determining convergence. As the absorption term appears with both $E^{n,\ell}$ and $E^{n,\ell+1}$, convergence is required for energy conservation to be preserved (see Sec. 2.5).

2.3. Introduction to smoothed particle hydrodynamics

In this section, the standard SPH derivatives needed for the thermal radiative transfer approximation are derived. For a more complete review of the SPH approximation, see Ref. [1].

Smoothed particle hydrodynamics involves interpolation of fields using kernels, which are functions centered at interpolation points. The initial assumption needed is that SPH kernels approximate delta functions, or $W\left(x - x', h\right) \to \delta\left(x - x'\right)$ as $h \to 0$, where h is the smoothing parameter that determines the width of the kernels,

$$\begin{aligned} g(x) &= \int_V \delta\left(x - x'\right) g\left(x'\right) dV' \\ &\approx \int_V W\left(x - x', h\right) g\left(x'\right) dV'. \end{aligned} \tag{21}$$

This also means that the integral of the kernel should be equal to one,

$$\int_V W\left(x-x',h\right)dV'=1. \tag{22}$$

In practice, the h can depend on both x and x'. The second assumption is that a set of kernels in space can be used to form a quadrature, with abscissas at the kernel centers $\boldsymbol{x}_i$ and weights equal to the kernel volume V_i. With these two assumptions, the kernels can be used to interpolate a function,

$$\begin{aligned}\langle g\left(x\right)\rangle &= \int_V W\left(x-x',h\right)g\left(x'\right)dV' \\ &\approx \sum_j V_j W\left(x-x_j,h\right)g_j.\end{aligned} \tag{23}$$

Here g_j is the function evaluated at point j, $g_j=g\left(x_j\right)$, and $\langle\cdot\rangle$ indicates an interpolated quantity. The interpolant is used to calculate derivatives of the field. This interpolant does not have the Kronecker delta property,

$$\langle g\left(x\right)\rangle_i=\sum_j V_j W\left(x_i-x_j,h\right)g_j\neq g_i. \tag{24}$$

To approximate a derivative in SPH, another three properties are needed from the kernel: that the kernel does not intersect a boundary, that the derivative of the kernel is antisymmetric in $\boldsymbol{x}$ and $\boldsymbol{x}'$, and that the integral of the derivative of the kernel is zero. With these approximations, the derivative of a function can be approximated as

$$\begin{aligned}\left\langle\partial_x^\alpha g\left(x\right)\right\rangle &= \int_V W\left(x-x',h\right)\partial_{x'}^\alpha g\left(x'\right)dV' \\ &= -\int_V \partial_{x'}^\alpha W\left(x-x',h\right)g\left(x'\right)dV' \\ &= \partial_x^\alpha\int_V W\left(x-x',h\right)g\left(x'\right)dV' - g\left(x\right)\partial_x^\alpha\int_V W\left(x-x',h\right)dV' \\ &\approx \sum_j V_j\left(g_j-g\left(x\right)\right)\partial_x^\alpha W\left(x-x_j,h\right).\end{aligned} \tag{25}$$

Note that because of the added $g\left(x\right)$ term (which equals zero in integral form due to the derivative), this approximation of the derivative goes to zero for a constant function.

For a diffusion-like problem, a second-order series expansion for $g\left(x\right)$ about x' and $g\left(x'\right)$ about x,

$$\partial_{x'}^\alpha g\left(x'\right)\approx\frac{x^\alpha-x^{\alpha,\prime}}{\left(x^\beta-x^{\beta,\prime}\right)\left(x^\beta-x^{\beta,\prime}\right)}\left[g\left(x'\right)-g\left(x\right)\right], \tag{26}$$

can be used to produce a commonly-used second-order approximation to the second derivative [1],

$$\begin{aligned}\left\langle\partial_x^\alpha\left[k\left(x\right)\partial_x^\alpha g\left(x\right)\right]\right\rangle &= \int_V W\left(x-x',h\right)\partial_{x'}^\alpha\left[k\left(x'\right)\partial_{x'}^\alpha g\left(x'\right)\right]dV' \\ &= -\int_V k\left(x'\right)\partial_{x'}^\alpha W\left(x-x',h\right)\partial_{x'}^\alpha g\left(x'\right)dV' \\ &= \partial_x^\alpha\int_V k\left(x'\right)W\left(x-x',h\right)\partial_{x'}^\alpha g\left(x'\right)dV' + k\left(x\right)\partial_x^\alpha g\left(x\right)\partial_x^\alpha\int_V W\left(x-x',h\right)dV' \\ &= \int_V\left[k\left(x\right)\partial_x^\alpha g\left(x\right)+k\left(x'\right)\partial_{x'}^\alpha g\left(x'\right)\right]\partial_x^\alpha W\left(x-x',h\right)dV' \\ &\approx \int_V\left[k\left(x\right)+k\left(x'\right)\right]\left[g\left(x\right)-g\left(x'\right)\right]\frac{x^\alpha-x^{\alpha,\prime}}{\left(x^\beta-x^{\beta,\prime}\right)\left(x^\beta-x^{\beta,\prime}\right)}\partial_x^\alpha W\left(x-x',h\right)dV'\end{aligned}$$

$$\approx \sum_j V_j \left(k\left(x\right)+k_j\right)\left(g\left(x\right)-g_j\right)\frac{x^\alpha - x_j^\alpha}{\left(x^\beta - x_j^\beta\right)\left(x^\beta - x_j^\beta\right)}\partial_x^\alpha W\left(x-x_j,h\right). \tag{27}$$

Like the first derivative approximation, the second derivative is zero for a constant function because the g terms cancel.

When discretizing an equation in SPH, the equation is first multiplied by the kernel $W\left(x-x',h\right)$ and integrated, similar to the finite element method. The distinction is that the interpolant is only used to calculate derivatives. The terms without derivatives are approximated using the definition of the interpolant,

$$\langle g\left(x\right)\rangle = \int_V W\left(x-x',h\right) g\left(x'\right) dV' \approx g\left(x\right). \tag{28}$$

The terms with derivatives are approximated as derivatives of the interpolant, as in Eq. (25). The final step in an SPH discretization is to add constraints to match the free variables in the equations. This can be done by multiplying the equations by a delta function $\delta\left(x-x_i\right)$ and integrating, or equivalently, evaluating the functions at $x=x_i$. This results in the fully-discrete approximations to Eqs. (23), (25), and (27),

$$\langle g\left(x\right)\rangle_i \approx \sum_j V_j W_{ij} g_j, \tag{29a}$$

$$\left\langle \partial_x^\alpha g\left(x\right)\right\rangle_i \approx \sum_j V_j \left(g_j - g_i\right)\partial_{x_i}^\alpha W_{ij}, \tag{29b}$$

$$\left\langle \partial_x^\alpha \left[k\left(x\right)\partial_x^\alpha g\left(x\right)\right]\right\rangle_i \approx \sum_j V_j \left(k_i + k_j\right)\left(g_i - g_j\right)\frac{x_{ij}^\alpha}{x_{ij}^\beta x_{ij}^\beta}\partial_{x_i}^\alpha W_{ij}, \tag{29c}$$

where

$$x_{ij}^\alpha = x_i^\alpha - x_j^\alpha, \tag{30a}$$

$$W_{ij} = W\left(x_{ij},h\right), \tag{30b}$$

$$\partial_{x_i}^\alpha W_{ij} = \partial_{x_i}^\alpha W\left(x_{ij},h\right). \tag{30c}$$

The smoothing length h connects the analytic kernel in Eq. (32c) with the SPH kernels,

$$W\left(x-x',h\right) = \psi\left(\frac{\sqrt{\left(x^\alpha - x^{\alpha,\prime}\right)\left(x^{\alpha,\prime} - x^{\alpha,\prime}\right)}}{h}\right). \tag{31}$$

In practice, the smoothing length is not constant and instead has discrete values at the SPH nodes. To retain symmetry in the derivatives [such that $\partial_{x_i}^\alpha W\left(x_i - x_j,h\right) = \partial_{x_j}^\alpha W\left(x_j - x_i,h\right)$], the kernel values are taken to be an average of the evaluations using these two smoothing lengths,

$$W_{ij} = \frac{1}{2}\left[W\left(x_{ij},h_i\right) + W\left(x_{ij},h_j\right)\right] \tag{32a}$$

$$\partial_{x_i}^\alpha W_{ij} = \frac{1}{2}\left[\partial_{x_i}^\alpha W\left(x_{ij},h_i\right) + \partial_{x_i}^\alpha W\left(x_{ij},h_j\right)\right]. \tag{32b}$$

The Wendland functions [37] are one example of a kernel that can be used in SPH. The Wendland C4 kernel is used here,

$$W_{\text{wendland}}\left(x_{ij},h\right) = \begin{cases} k\left(1-r\right)^5\left(8r^2+5r+1\right), & r \equiv x_{ij}/h \le 1, \\ 0, & \text{otherwise}, \end{cases} \tag{32c}$$

with a dimensionally-dependent normalization constant k that is chosen such that Eq. (22) is satisfied. The choice of interpolation kernel is of course arbitrary for meshfree methods such as these, and many have been used over the years. Wendland kernels are common in many modern SPH studies (e.g. [38,39]), but this choice is not necessarily unique.

Note in this section the per point volume V_j has been used (such as in Eq. (23)), leading to explicitly volume weighted relations throughout. SPH does not define a volume element per point as such, so in this paper the volume is defined as $V_j = m_j/\rho_j$. It is common in the SPH literature to substitute this relation for V_j and then rearrange terms to remove the density from inside the summation, such that only the fixed (and well defined) mass per point remains (see for instance the discussion in Sec. 2.2 of [1]). In this work the volume remains inside the second derivative, which may affect the accuracy of the method in regions of high density contrast. This definition is consistent with the diffusion derivative in Refs. [12] (where the mass of the particles is constant) and [1] (where the mass is variable). It is possible these results might be improved by rearranging such definitions analogously to how first derivatives are typically handled, but such an investigation is left to follow-on studies.

2.4. Spatial discretization

To perform the spatial discretization, the material and radiation energy equations [Eqs. (18)] are multiplied by $W\left(x_i - x', h\right)$ and integrated,

$$\left\langle \frac{\rho}{\Delta t}\left(e^{n,\ell+1} - e^{n-1}\right) + c\sigma_a B^{n,\ell+1} - c\sigma_a E^{n,\ell+1} - Q_e^n \right\rangle_i = 0, \tag{33a}$$

$$\left\langle \frac{1}{\Delta t}E^{n,\ell+1} - \partial_x^\alpha \frac{c\lambda}{\sigma_t}\partial_x^\alpha E^{n,\ell+1} + c\sigma_a f E^{n,\ell+1} \right\rangle_i = \left\langle \frac{1}{\Delta t}E^{n-1} + c\sigma_a B^{n,\ell} - (1-f)\,c\sigma_a E^{n,\ell} + Q_E^n \right\rangle_i, \tag{33b}$$

where $\langle\cdot\rangle$ is the interpolant notation as defined in Sec. 2.3. The terms not involving derivatives can be approximated using Eq. (28), e.g.

$$\left\langle \frac{\rho}{\Delta t}e^{n-1} \right\rangle \approx \frac{\rho_i}{\Delta t}e_i^{n-1}, \tag{34}$$

$$\left\langle c\sigma_a f E^{n,\ell+1} \right\rangle_i \approx c\sigma_{a,i} f_i E_i^{n,\ell+1}. \tag{35}$$

The second derivative in the radiation energy equation can be approximated using Eq. (27),

$$\left\langle -\partial_x^\alpha D\,(x)\,\partial_x^\alpha E\,(x) \right\rangle \approx -\sum_j V_j\left(D_i + D_j\right)\left(E_i - E_j\right)\frac{x_{ij}^\alpha}{x_{ij}^\beta x_{ij}^\beta}\partial_{x_i}^\alpha W_{ij}, \tag{36}$$

with the diffusion coefficient

$$D_i = \frac{c\lambda_i}{\sigma_{t,i}}. \tag{37}$$

With these approximations, the material and radiation equations are

$$\frac{\rho_i}{\Delta t}\left(e_i^{n,\ell+1} - e_i^{n-1}\right) + c\sigma_{a,i}B_i^{n,\ell+1} - c\sigma_{a,i}E_i^{n,\ell+1} - Q_{e,i}^n = 0, \tag{38a}$$

$$\begin{aligned}\frac{1}{\Delta t}E_i^{n,\ell+1} - \sum_j V_j\left(D_i + D_j\right)\left(E_i^{n,\ell+1} - E_j^{n,\ell+1}\right)\frac{x_{ij}^\alpha}{x_{ij}^\beta x_{ij}^\beta}\partial_{x_i}^\alpha W_{ij} + c\sigma_{a,i}f_i E_i^{n,\ell+1} \\ = \frac{1}{\Delta t}E_i^{n-1} + c\sigma_{a,i}B_i^{n,\ell} - (1-f_i)\,c\sigma_{a,i}E_i^{n,\ell} + Q_{E,i}^n.\end{aligned} \tag{38b}$$

The material energy equation is independent for each point i, while the radiation energy equation for point i linearly couples to the radiation energy from nearby nodes. For more information on how these equations are solved, see Sec. 3.2.

2.5. Conservation

The coupled material and radiation equations [Eqs. (38)] are conservative in energy to the tolerance of the nonlinear iteration process once converged. The quantity that is conserved is the total energy over all points, which is the material energy plus the radiation energy,

$$\sum_i \left(m_i e_i + V_i E_i\right) = \text{const.} \tag{39}$$

At convergence, $e^{n,\ell+1} \approx e^{n,\ell}$ and $E^{n,\ell+1} \approx E^{n,\ell}$, which results in the simplified equations

$$\frac{\rho_i}{\Delta t}\left(e_i^n - e_i^{n-1}\right) + c\sigma_{a,i}B_i^n - c\sigma_{a,i}E_i^n = Q_{e,i}^n, \tag{40a}$$

$$\frac{1}{\Delta t}\left(E_i^n - E_i^{n-1}\right) - \sum_j V_j\left(D_i + D_j\right)\left(E_i^n - E_j^n\right)\frac{x_{ij}^\alpha}{x_{ij}^\beta x_{ij}^\beta}\partial_{x_i}^\alpha W_{ij} + c\sigma_{a,i}E_i^n - c\sigma_{a,i}B_i^n = Q_{E,i}^n. \tag{40b}$$

Adding the two equations, multiplying by V_i, and summing over i results in

$$\sum_i \left[m_i\left(e_i^n - e_i^{n-1}\right) + V_i\left(E_i^n - E_i^{n-1}\right)\right] = \Delta t\sum_i\left(Q_{e,i}^n + Q_{E,i}^n\right). \tag{41}$$

Because the diffusion spatial derivative is antisymmetric about i and j, it disappears under summation over both i and j. This final equation says that any gains or losses in the total energy are as a result of specified sources. At equilibrium and absence external sources, both the material and the radiation equations reduce to an equilibrium absorption-emission rate at every point x_i, which is $E_i = B_i$.

3. Methodology

The thermal radiative transfer methods described here are implemented within the open-source SPH code Spheral, described at https://wci.llnl.gov/simulation/computer-codes/spheral and publicly available at https://github.com/jmikeowen/spheral, although the radiative transfer methods are not available in the open source version. For access to the full code, including thermal radiative transfer and input scripts for the problems presented in this paper, please contact the authors. Spheral is written in C++ with a Python interface, which allows for simple addition of new physics in either programming language. The opacities, flux limiters, and equations of state can be chosen arbitrarily for subsets of the SPH points as needed, allowing problems with any number of distinct materials to be studied.

3.1. Meshless implementation

In the succeeding examples Spheral's default method [40] for computing the smoothing scale per point (h_i) is used with the C4 Wendland kernel [Eq. (32c)]. The target radius of support is 4 points, i.e., the local smoothing scale for each point is chosen to be 4 times the local particle spacing. The smoothing scale algorithm from [40] is iterated until the desired support for each point is achieved during problem initialization. Since the points in these examples are not moving, the smoothing scale is unchanged after this initialization.

Boundary conditions are handled with ghost nodes, which provide sufficient support for the internal nodes and allow the boundary terms in SPH to be neglected. The ghost points can be set to have constant values independent of internal nodes or to represent an internal node. For reflective or periodic boundaries, the points adjacent to the boundary are copied across the boundary. The domain decomposition is done similarly, where all neighboring points for those in the subdomain for a processor are copied as ghost points.

3.2. Material and radiation energy solve

The iterative process in Algorithm 1 [24] can be written in terms of operator matrices as

$$\begin{bmatrix} e^{\ell+1} \\ E^{\ell+1} \end{bmatrix} = \begin{bmatrix} \mathbb{M}^{-1} & 0 \\ 0 & \mathcal{I} \end{bmatrix} \begin{bmatrix} \mathcal{R} & \mathcal{A} \\ 0 & \mathcal{I} \end{bmatrix} \begin{bmatrix} \mathcal{I} & 0 \\ 0 & \mathcal{D}^{-1} \end{bmatrix} \begin{bmatrix} \mathcal{I} & 0 \\ \mathbb{N} & \mathcal{S} \end{bmatrix} \begin{bmatrix} e^{\ell} \\ E^{\ell} \end{bmatrix}, \tag{42}$$

with the operators defined by

$\mathbb{M}^{-1}(P)$ Solve the nonlinear material equation, given a source P_i,

$$\frac{\rho_i}{\Delta t}\left(e_i - e_i^{n-1}\right) + c\sigma_{a,i} a T_i^4 = P_i, \tag{43}$$

for each e_i,

$\mathcal{D}^{-1}(P)$ Solve the diffusion equation, given a source P_i,

$$\left(\frac{1}{\Delta t} + c\sigma_{a,i} f_i\right) E_i - \sum_j V_j \left(D_i + D_j\right)\left(E_i - E_j\right) \frac{x_{ij}^{\alpha}}{x_{ij}^{\beta} x_{ij}^{\beta}} \partial_{x_i}^{\alpha} W_{ij} = P_i, \tag{44}$$

for all E_i,

$\mathcal{S}(E)$ Calculate the radiation diffusion source, $\frac{1}{\Delta t} E_i^{n-1} - (1 - f_i) c\sigma_{a,i} E_i + Q_{E,i}$,

$\mathbb{N}(e)$ Calculate the emission of radiation from the material, $c\sigma_{a,i} a T_i^4$,

$\mathcal{A}(E)$ Calculate the radiation energy absorption, $c\sigma_{a,i} E_i$,

$\mathcal{R}(e)$ Set the material energy source, $Q_{e,i}^n$,

and the identity operator $\mathcal{I}$. This simplifies the addition of new physics, reduces code duplication, and allows testing of each operator independently. Note that $\mathbb{M}^{-1}$ and $\mathbb{N}$ are nonlinear operators, and should not be mistaken for matrices. The operators $\mathcal{D}^{-1}$, $\mathcal{S}$, and $\mathcal{A}$ are linear, but in practice, they are not explicitly formed into matrices. The application of the combined operator in Eq. (42) is equivalent to a single outer iteration in Algorithm 1. The opacities and other material data (σ_a, σ_s, D, f, λ, and c_v) are calculated at the start of the time step and held constant within the time step.

The material energy solve in Eq. (43) is done independently for each point using Newton's method, as shown in Eq. (19). Defining the function and Jacobian for the material energy solve as

$$u(e_i) = \frac{\rho}{\Delta t}\left(e_i - e^{n-1}\right) + c\sigma_a a T^4 - P, \tag{45a}$$

$$J_{m,e}(e) = \frac{\rho}{\Delta t} + \frac{4c\sigma_a a T^3}{c_v}, \tag{45b}$$

the material energy is solved iteratively as

$$e_i^{k+1} = e_i^k - J_{m,e}^{-1}\left(e_i^k\right) u\left(e_i^k\right) \tag{45c}$$

until converged, where k is the Newton iteration index. As the call to an external equation of state can be expensive, the temperature is updated for all points simultaneously, followed by an update of the material energy for each point independently. The iterative process in Eq. (45c) proceeds until convergence each time the $\mathcal{M}^{-1}$ operator is called.

The radiation energy solve in Eq. (44) is done using the Hypre BoomerAMG preconditioner with GMRES [32]. Because the material properties (opacities, specific heats, hydrodynamic variables) are held constant within a time step, the preconditioner can be initialized once at the start of each time step and then reused each time the $\mathcal{D}^{-1}$ operator is called within the time step. The radiation energy E^ℓ is used as an initial guess for the GMRES solver when calculating $E^{\ell+1}$, which reduces the number of GMRES iterations as the solution nears convergence, as is discussed in Sec. 4.3.

3.3. Time step choice

Due to the implicit solve, the time step is updated not based on the propagation speed of the radiation, but instead based on the observed change in radiation energy over a time step. This is a heuristic for the stability and accuracy of one Newton step. The idea is to limit the fractional change in the material and radiation energies to some finite value and increase or decrease the time step according to the change from the previous time step. For example, for the material energy, the fractional change in energy is calculated as

$$\eta_e = \max_i \left(\frac{\left| e_i^n - e_i^{n-1} \right|}{e_i^n + \eta_e^{\text{target}} \bar{e}^n} \right), \tag{46}$$

where η_e^{target} is the target fractional change ($\eta_e^{\text{target}} = 0.05$ for the problems in this paper) and $\bar{e}^n$ is the volume-averaged energy,

$$\bar{e}^n = \frac{\sum_i e_i^n V_i}{\sum_i V_i}. \tag{47}$$

The $\bar{e}^n$ in the denominator of the fractional change prevents points with very small radiation energy from dominating the time step when changing a small magnitude relative to the other points in the problem. Given the fractional change over the previous time step, a proposed time step is calculated as

$$\Delta t_e^{n+1} = \Delta t^n \left(\frac{\eta_e^{\text{target}}}{\eta_e} \right)^{1/2}. \tag{48}$$

The fractional change in energy [Eq. (46)] depends on the energy being nonzero somewhere in the problem. If it is anticipated that the energy might be zero everywhere in the problem, a small number (e.g. 10^{-15}) can be added to the denominator to prevent division by zero.

The same is process is done for the radiation energy E, and the time step is chosen to be the more restrictive of these, $\Delta t^{n+1} = \min\left(\Delta t_e^{n+1}, \Delta t_E^{n+1}\right)$, within the minimum and maximum time steps specified by the user. For more information on time stepping strategies for thermal radiative transfer with diffusion, including the one used here, see Ref. [41].

4. Results

The results include three problems. The first is an infinite medium equilibrium test, which is designed to show that the material and radiation energies come to equilibrium at the correct rate, testing the time discretization, emission, and absorption. The second is the Su-Olson Marshak wave, which simulates the diffusion of a planar radiation source into a vacuum, additionally testing the diffusion rate of the radiation. The final problem is a manufactured solution that extends the results to two and three dimensions. The tolerances used for each of these problems are listed in Table 1, with the inner tolerances referring to the convergence metric for ending the Newton solve for the material energy and the GMRES solve for the radiation energy and the outer tolerances used for ending the nonlinear elimination iteration process (see Sec. 3.2).

4.1. Infinite medium equilibrium test

The first problem involves a single material in an infinite medium in which the material and radiation energies are initially out of equilibrium, similar to the tests performed in Refs. [7,8]. The units of length, time, temperature, and mass are chosen such that the absorption opacity σ_a, speed of light c, black body constant a, and ratio of proton mass to the

Table 1
Convergence tolerances for the results. Then inner tolerance is for the independent radiation and material energy solves, while the outer tolerance is for the combined solve.

Problem	Inner		Outer	
	Material	Radiation	Material	Radiation
Infinite medium	10^{-14}	10^{-14}	10^{-12}	10^{-12}
Marshak wave	10^{-12}	10^{-12}	10^{-8}	10^{-8}
Manufactured problem	10^{-12}	10^{-12}	10^{-8}	10^{-8}

Table 2
Initial conditions for infinite medium problem for two cases, one starting with a high thermal temperature and low radiation temperature and one with the temperatures reversed. See Sec. 4.1 for units.

Case	e_0	E_0	$T_{e,0}$	$T_{r,0}$	Δt_{init}
Hot material	1.0	10^{-16}	1.0	10^{-4}	10^{-20}
Hot radiation	10^{-4}	1.0	10^{-4}	1.0	10^{-7}

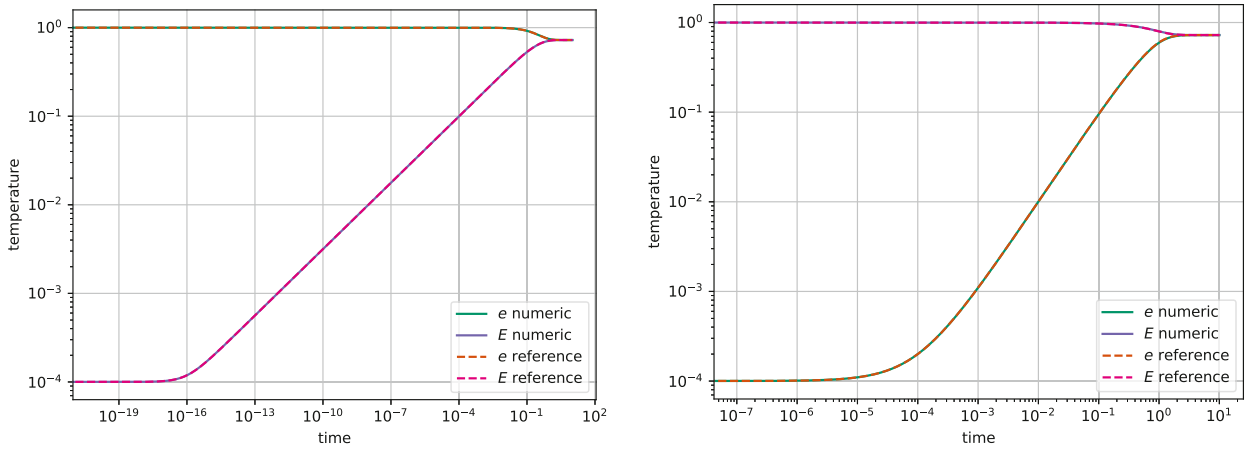

(a) Hot material at initial time

(b) Hot radiation at initial time

Fig. 1. Comparison of reference and numerical results for the infinite medium problem. The time step is fixed at $\Delta t = 0.0001$.

Boltzmann constant, m_p/k_B, are all one. The equation of state is chosen to be an ideal gas [Eq. (3)], which in these units is defined as

$$T = (\gamma - 1)\,\mu e. \tag{49}$$

The problem can be written in the simplified unit system as a system of two ordinary differential equations,

$$\rho \frac{\partial e}{\partial t} = E - (\alpha e)^4, \tag{50}$$

$$\frac{\partial E}{\partial t} = -E + (\alpha e)^4. \tag{51}$$

These equations are solved using a fifth-order Radau IIA integrator [42] for comparison to the results given by the code.

The problem is run for two different cases, both of which have $(\gamma - 1)\,\mu = 1$ and a density of $\rho = 1$, and in each case, the simulation proceeds until $t_{end} = 10$, which allows the material and radiation energies to reach equilibrium. The first case starts with hot material and cold radiation, while the second starts with cold material and hot radiation, as shown in Table 2. The time step is allowed to increase by up to an order of magnitude per time step, up to the limit set by the changing material and radiation energies, with a hard cap of $\Delta t_{max} = 0.1$ (see Sec. 3.3).

The first and second cases take, respectively, 779 and 155 time steps to reach the goal time. The results are shown in Fig. 1. The reference and numeric solutions agree well for both problems. The L_1 relative error for this problem is calculated with an integral in time,

$$L_1 \text{ error} = \frac{\int_0^{t_{end}} |T_{\text{ref}} - T_{\text{num}}|\,dt}{\int_0^{t_{end}} T_{\text{ref}} dt}, \tag{52}$$

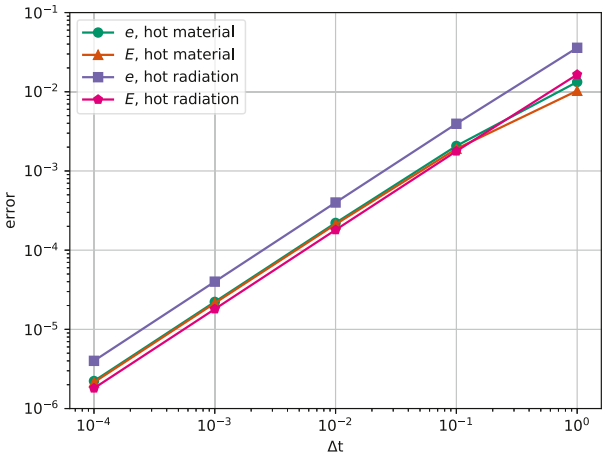

Fig. 2. Convergence of the numerical solution for the infinite medium problem to the reference solution with decreasing time step. The error is calculated using Eq. (52).

using Simpson's rule evaluated at the time steps. The error between the reference and numeric solutions for the first case (with hot material) is 3.32×10^{-4} for the material temperature and 2.55×10^{-4} for the radiation temperature. The error calculated in the same way for the second case (with hot radiation) is 1.22×10^{-3} for the material temperature and 6.21×10^{-4} for the radiation temperature. For a fixed time step Δt, the error decreases linearly with Δt as expected, as shown in Fig. 2.

The relative error between the initial and final energies ranges from 1.11×10^{-15} (hot radiation) and 4.44×10^{-16} (hot material) for $\Delta t = 0.1$ to 4.22×10^{-13} (hot radiation) and 5.53×10^{-13} (hot material) for $\Delta t = 0.0001$, which is of the correct order given the outer tolerance of 10^{-12} and inner tolerance of 10^{-14} (Table 1).

4.2. Su-Olson Marshak wave

The second problem is a Marshak planar wave as described in Ref. [43]. The problem consists of a reflecting plane at $x = 0.0$ and a radiation source from $0 \leq x \leq x_0$ that is turned on for $0 \leq \tau \leq \tau_0$, where x is a scaled distance and τ is a scaled time (z is used in the paper for physical distance). The problem is started with a material and radiation energy of 10^{-5} so the heat capacity (an analytic $c_v \propto T^3$) is nonzero. The equation of state from the original paper [43] is

$$e = \frac{4a}{\epsilon} T^4, \tag{53}$$

where ϵ is a time scaling factor. The units for the problem are chosen such that $\sigma_t = 1$, $\epsilon c = 1$, and $a = 1$, which makes the scaled units referenced in the paper equal to the physical units ($x = z$ and $\tau = t$). The solution to the problem is semianalytic, and involves evaluating integrals to high precision over $\eta \in [0, 1]$ for each spatial point at each time. For these results, due to the complicated structure of the solution near $\eta = 1$, a quadrature is first generated in $\xi \in [-1, 1]$ and then transformed into η via the relation

$$\eta = \frac{1}{\ell} \ln\left(\frac{1}{2}\left(1 - \xi + e^{\ell}\,(1 + \xi)\right)\right), \tag{54}$$

in which the transformation becomes linear as $\ell \to 0$ and concentrates more points near $\eta = 1$ as ℓ increases. A 5000-point Gauss-Legendre quadrature with $\ell = 3$ works well for the specific problem considered below. The numerical result at the end time is compared to this semianalytic result using an L_1 error,

$$L_1 \text{ error} = \frac{\sum_i \left| e_i - e_i^{\text{semianalytic}} \right|}{\sum_i e_i^{\text{semianalytic}}}, \tag{55}$$

which differs from the standard approach of comparison to specific x and τ values tabulated in the paper.

The parameters used for these results include an absorption fraction of $c_a = 0.5$, a time scaling factor of $\epsilon = 1.0$, a radiation source extent of $x_0 = 0.5$, and a scaled time at which the source is turned off of $\tau_0 = 10.0$. The problem is run until $\tau = 100.0$. The spatial extent of the problem is $0 \leq x \leq 100$.

The time evolution of the semianalytic and numeric solutions is shown in Fig. 3. The spatial convergence results are shown in Fig. 4 for three different time steps. The code converges to the semianalytic result with second-order accuracy spatially as the point spacing decreases and with first-order accuracy temporally as the time step decreases, as expected based on SPH spatial interpolation and backward Euler time integration.

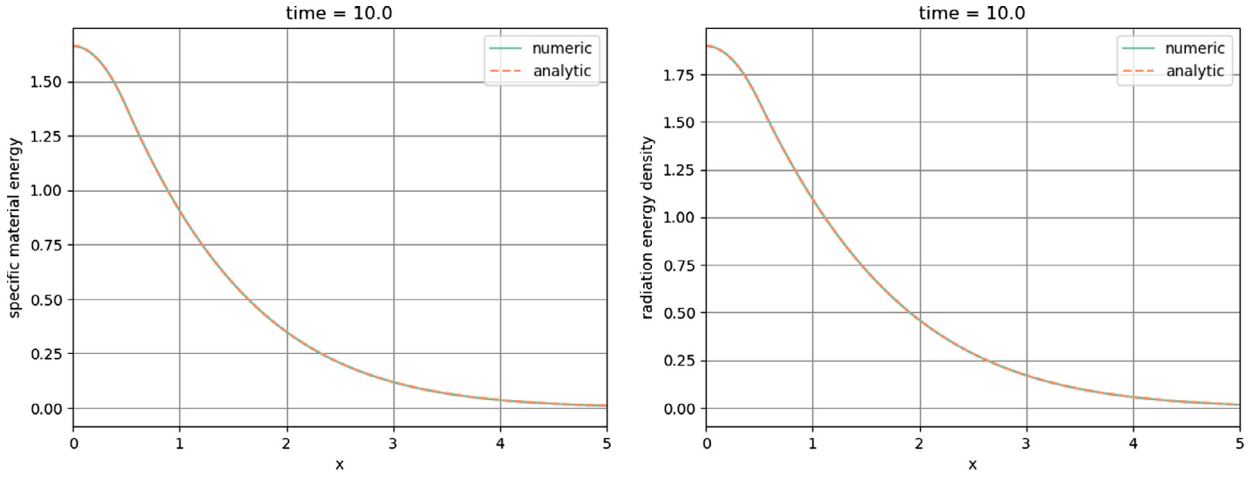

(a) Material energy (b) Radiation energy

Fig. 3. The numeric and semianalytic solutions to the Marshak wave problem at $t = 10.0$. This figure is also available as a video.

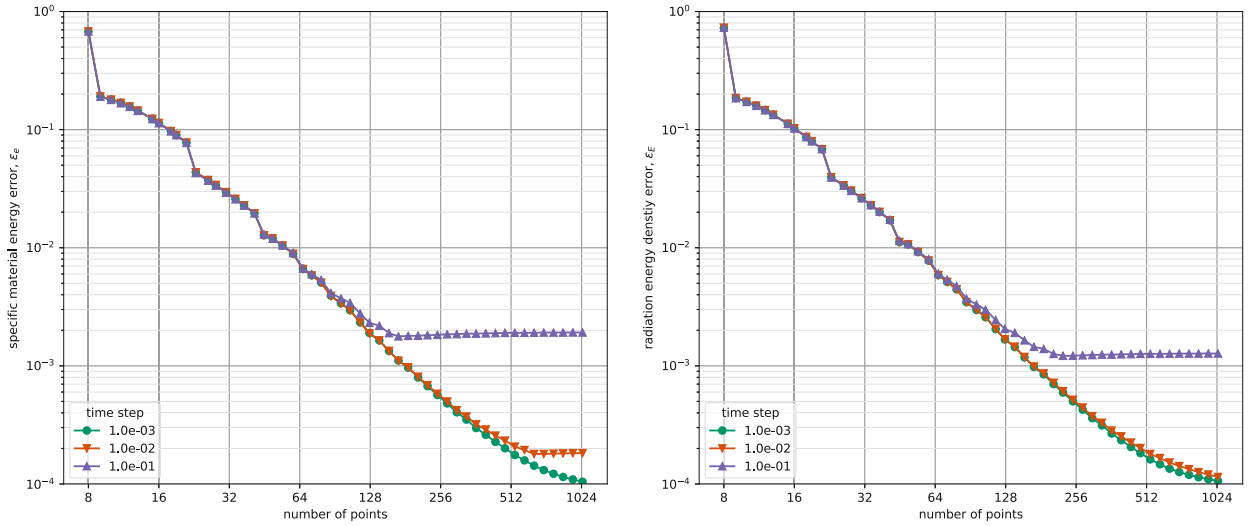

(a) Material energy (b) Radiation energy

Fig. 4. Convergence of the numeric solution to the semianalytic solution for the Marshak wave with an increasing number of spatial points for three time step values. The error is calculated using Eq. (55).

4.3. Manufactured solution for material-radiation coupling

This problem tests the material-radiation coupling using the method of manufactured solutions (MMS). To apply MMS to Eqs. (38), solutions for e and E are chosen for the equations,

$$e_m = e_0 \left[1.2 + \prod_{\alpha=1}^{\dim} \cos\left(2\pi \frac{x_\alpha - v_m t}{d_m} \right) \right], \tag{56a}$$

$$E_m = E_0 \left[1.2 + \prod_{\alpha=1}^{\dim} \cos\left(2\pi \frac{x_\alpha + v_m t}{d_m} - \omega_m \right) \right], \tag{56b}$$

with $e_0 = 10^{13}$ ergs·g^{-1}, $E_0 = 7a\,(e_0/c_v)^4$ ergs·cm^{-3}, $v_m = 5 \times 10^9$ cm·s^{-1}, $d_m = 5$ cm, and $\omega_m = 1/16$. The opacities are set to constant values of $\sigma_a = 0.05$ cm^{-1} and $\sigma_s = 0.95$ cm^{-1}. These solutions are inserted into the non-discretized equations [Eqs. (1a) and (7)] to calculate sources, Q_e and Q_E. The solutions are chosen such that the magnitude of the individual terms in Eqs. (1a) and (7) is approximately equal, with the opposite time movement of the waves $\pm v$ allowing each individual piece of physics to dominate at certain times. The spatial extent of the problem is set to one full wavelength, or d_m in each

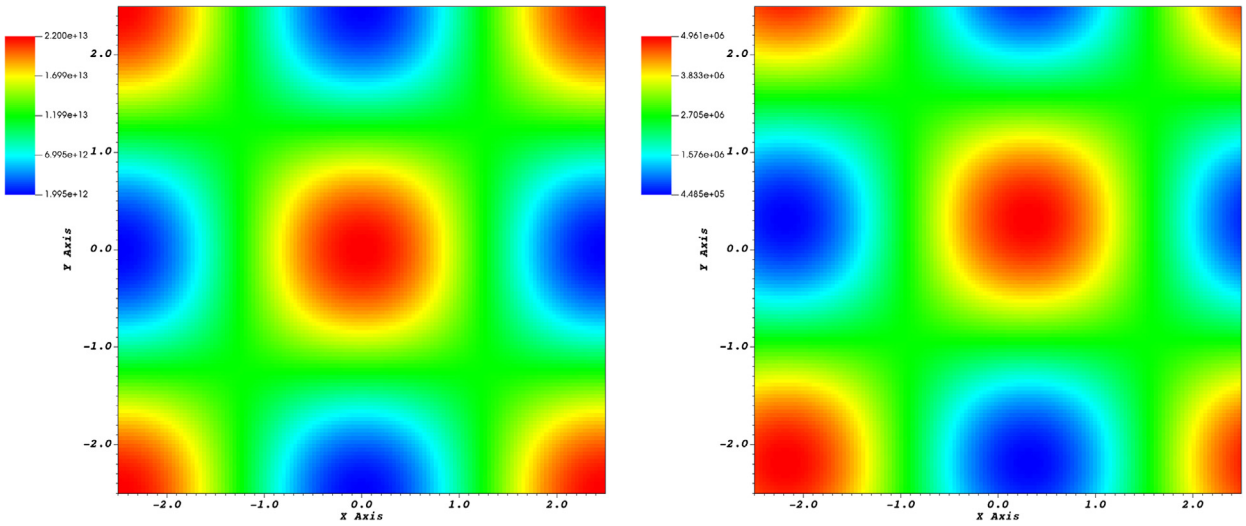

(a) Material energy (b) Radiation energy

Fig. 5. The numeric solution to the manufactured problem in 2D for 128^2 points after one cycle. This figure is also available as a video. (For interpretation of the colors in the figure(s), the reader is referred to the web version of this article.)

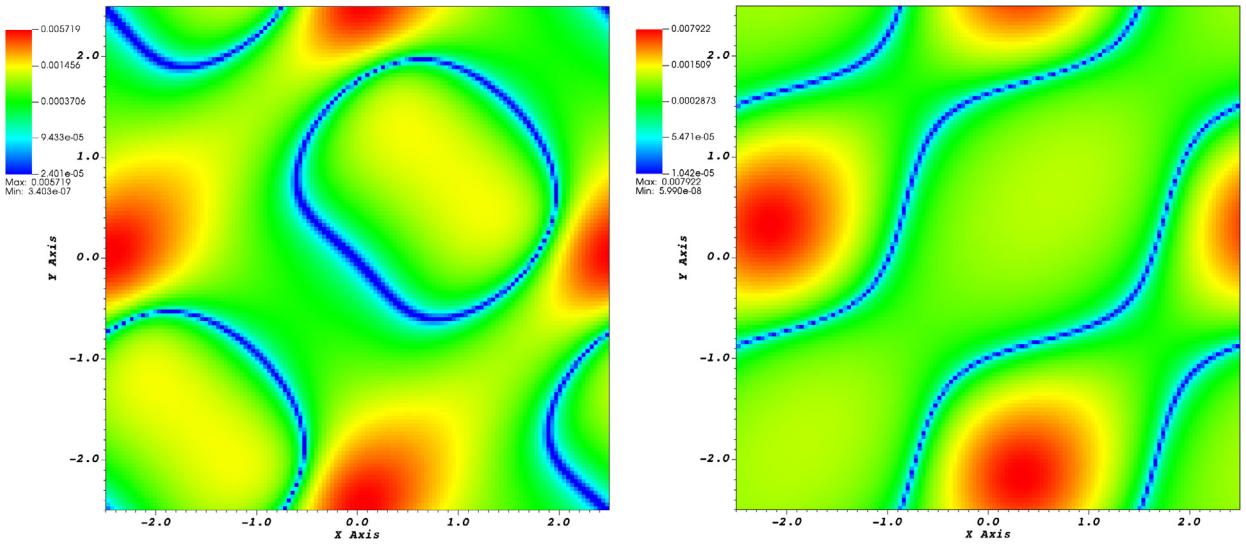

(a) Material energy (b) Radiation energy

Fig. 6. Pointwise relative error of the numeric solution to the manufactured problem at 10^{-9} s in 2D for 128^2 points.

dimension (to allow for periodic boundary conditions), and the problem is run for one cycle, or until $t_{end} = d_m/v_m$, using a time step of $\Delta t = t_{end}/1000$. At t_{end}, the numerical solution is compared to the analytic solution in Eqs. (56) to calculate the L_1 relative error,

$$L_1 \text{ error} = \frac{\sum_i \left| e_i - e_{m,i} \right|}{\sum_i e_{m,i}} \tag{57}$$

(with a similar equation for E). The ideal gas equation of state is used [Eq. (3)] with $\gamma = 5/3$ and $\alpha = 1$.

The solution for the problem with 128^2 points is shown in Fig. 5. At the end time, the solution should be equal to the initial condition. The relative error between the solution after one cycle (at 10^{-9} s) and the manufactured solution for the specific thermal energy and radiation energy density is shown in Fig. 6. The relative error is highest where the solution is lowest, with maxima of 0.006 for the specific material energy and 0.008 for the radiation energy. For much of the domain, the relative error is below 0.001 for both the material and radiation energy. At the end time, the relative difference between the starting and ending energy of the system is 1.67×10^{-12}, which indicates good energy conservation.

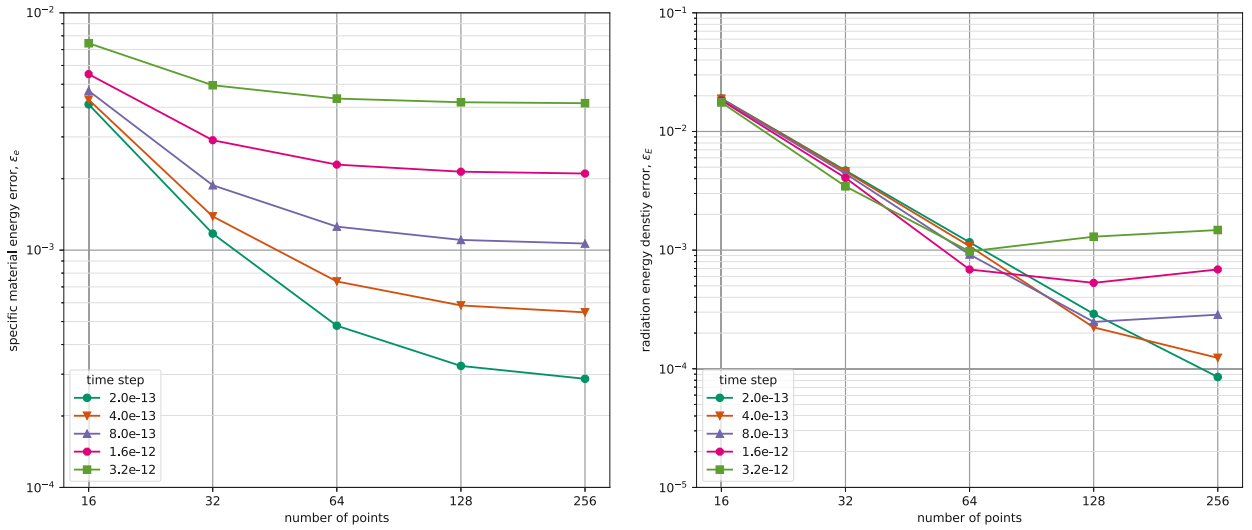

(a) Material energy (b) Radiation energy

Fig. 7. Convergence of the numeric solution to the manufactured problem for several time step values in 1D. The error is calculated using Eq. (57). Note that the material energy is more dependent on the time step for convergence than the radiation energy, and thus does not show the same second-order convergence for the time steps shown here.

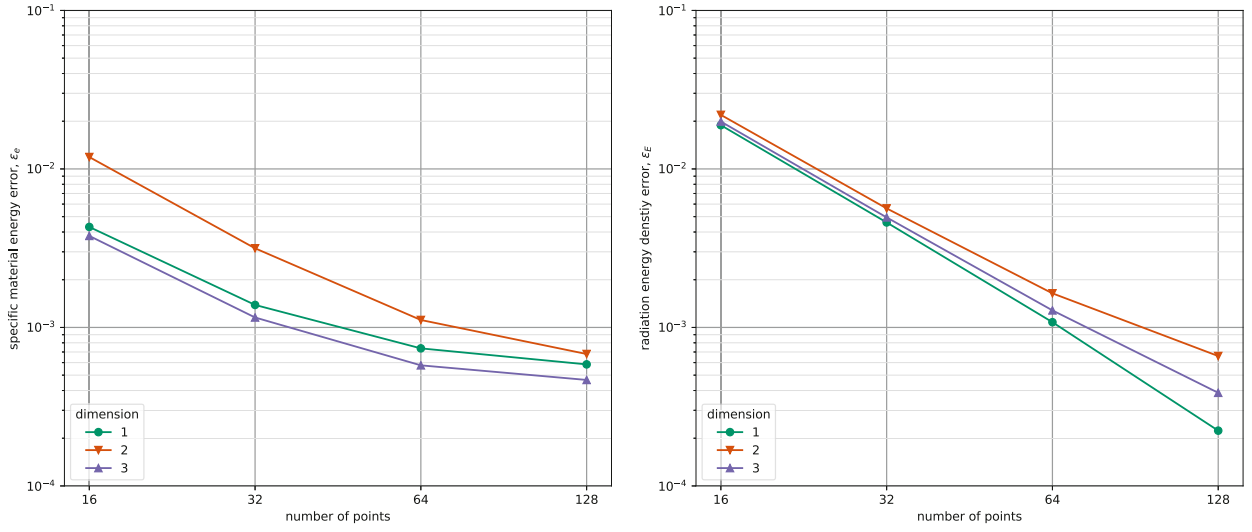

(a) Material energy (b) Radiation energy

Fig. 8. Convergence of the numeric solution to the manufactured problem in 1D, 2D, and 3D with a fixed time step of $\Delta t = 4 \times 10^{-13}$. The error is calculated using Eq. (57).

The L_1 error for the manufactured problem in 1D for several time step values is shown in Fig. 7. The numeric solution converges to the manufactured solution with second-order accuracy in space and first-order accuracy in time (again as expected). For a time step of 2×10^{-13}, the error in the radiation energy indicates second-order convergence for all values of point spacing. The error in the material energy, which only has spatial coupling through the radiation, is much more dependent on the time step for this problem than the radiation energy. As in the previous problems, the error decreases linearly with the time step, when not limited by the spatial error.

Based on the results in 1D, a time step of 4×10^{-13} is chosen for the comparison of 1D, 2D, and 3D results up to 128^d points (for the dimension d). The convergence results for 1D, 2D, and 3D are shown in Fig. 8. The 2D and 3D results have similar errors compared to the manufactured solution for similar spacing of points, although not identical due to differences in the interpolation functions for 2D and 3D, and also show second-order convergence when not limited by the time step.

Table 3
Timing for the manufactured problem in 3D.

Dimension	Points	Procs	Points/proc	GMRES/Outer	Outer/Step	Wall time (s)	Time×Proc/Point
2	256	36	7	3.66	3	59	8.29
	1,024	36	28	4.66	3	79	2.78
	4,096	36	113	3.33	3	261	2.29
	16,384	36	455	3.66	3	817	1.79
3	4096	36	113	3.66	3	815	7.21
	32,768	36	910	4.66	3	5,610	6.20
	262,144	288	910	3.33	3	7,660	8.41
	2,097,152	576	3,640	3.66	3	31,975	8.78

While the number of processors used for each case was not chosen to show scaling with a constant number of points per processor or a constant number of total points, the performance results in Table 3 show some general scaling trends. In 2D, the small number of points per processor means that communication costs dominate, and adding more points per each processor helps reduce that cost. In 3D, the cases with 910 points per processor show around a 74 percent efficiency when the number of points and processors are quadrupled. With many more points per processor than the other cases, the 2,097,152-point problem on 576 processors runs with a similar efficiency to the 262,144-point problem in 288 processors. Note that the 3D results take a long time to run due to the high level of support, up to several hundred neighbors per point.

The number of outer iterations per time step is governed for this problem by the tolerance. For the tolerance given in Table 1, the solver needed two outer iterations to converge (and a third to check for convergence) in each time step. The number of GMRES iterations per outer iteration is around 3-4 on average. At the start of a time step, when the guess for the material and radiation energies is based on the values from the previous time step, the number is generally higher, around 6-8. On the last outer iteration, the number of GMRES solves is 1, indicating that the guess from the previous iteration satisfies the diffusion equation.

The solution to the problem is the same at the start and end times, so despite adding and subtracting energy in certain regions of the problem, the initial and final energies should be equal. The relative error between the initial and final energy in 2D ranges from 6.35×10^{-14} for the 256 points to 1.69×10^{-12} for 16,384 points. For 3D, the relative error ranges from 1.33×10^{-13} for 4,096 points to 4.53×10^{-12} for 2,097,152 points. In both cases, the relative error is on the order of the tolerance for the radiation solve of 10^{-12} and much lower than the tolerance of the coupled radiation and material energy solve of 10^{-8}.

5. Conclusions and future work

The thermal radiative transfer equations with grey diffusion is discretized fully implicitly in time and solved using an efficient nonlinear elimination method that leads to fast convergence of the emission source. A standard SPH diffusion derivative is applied to the modified equations to form a fully discretized set of equations that are conservative in energy. The diffusion term is solved using optimized linear solvers, which permits good parallel efficiency.

The code is verified by comparison to three test problems with known solutions. The code gets the correct infinite medium behavior for either a hot material emitting radiation or a cold material absorbing radiation, with the expected first-order convergence in time. The results for a one-dimensional semianalytic Marshak wave problem are consistent with second-order spatial convergence. Finally, the code is run in 2D and 3D for a manufactured problem with sinusoidal radiation and material energy solutions traveling in opposite directions, which likewise exhibits second-order convergence in space and first-order convergence in time.

The diffusion discretization for SPH is stable and performs well, but lacks zeroth-order consistency. Other methods, such as reproducing kernel particle methods [44] and moving least squares particle hydrodynamics [4,5], do not lack the zeroth-order consistency and perform better near boundaries. Conservative reproducing kernel smoothed particle hydrodynamics is implemented in the SPH code used for these results [6], and a similar diffusion discretization would make the hydrodynamics and radiation discretizations consistent. Other discretizations would also make the application of vacuum or incoming radiation boundary conditions more feasible.

CRediT authorship contribution statement

Brody R. Bassett: Conceptualization, Methodology, Software, Validation, Visualization, Writing – original draft, Writing – review & editing. **J. Michael Owen:** Conceptualization, Project administration, Software, Supervision, Writing – review & editing. **Thomas A. Brunner:** Methodology, Supervision, Writing – review & editing.

Declaration of competing interest

The authors declare that they have no known competing financial interests or personal relationships that could have appeared to influence the work reported in this paper.

Acknowledgements

This work was performed under the auspices of The U.S. Department of Energy by Lawrence Livermore National Laboratory under Contract DE-AC52-07NA27344. This document was prepared as an account of work sponsored by an agency of the United States government. Neither the United States government nor Lawrence Livermore National Security, LLC, nor any of their employees makes any warranty, expressed or implied, or assumes any legal liability or responsibility for the accuracy, completeness, or usefulness of any information, apparatus, product, or process disclosed, or represents that its use would not infringe privately owned rights. Reference herein to any specific commercial product, process, or service by trade name, trademark, manufacturer, or otherwise does not necessarily constitute or imply its endorsement, recommendation, or favoring by the United States government or Lawrence Livermore National Security, LLC. The views and opinions of authors expressed herein do not necessarily state or reflect those of the United States government or Lawrence Livermore National Security, LLC, and shall not be used for advertising or product endorsement purposes. LLNL-JRNL-799713.

Appendix A. Supplementary material

Supplementary material related to this article can be found online at https://doi.org/10.1016/j.jcp.2020.109996.

References

[1] Joe J. Monaghan, Smoothed particle hydrodynamics, Rep. Prog. Phys. 68 (8) (2005) 1703.
[2] M.B. Liu, G.R. Liu, Smoothed particle hydrodynamics (SPH): an overview and recent developments, Arch. Comput. Methods Eng. 17 (1) (2010) 25–76.
[3] Joseph Peter Morris, A study of the stability properties of smooth particle hydrodynamics, Publ. Astron. Soc. Aust. 13 (1) (1996) 97–102.
[4] Gary A. Dilts, Moving-least-squares-particle hydrodynamics I: consistency and stability, Int. J. Numer. Methods Eng. 44 (8) (1999) 1115–1155.
[5] Gary A. Dilts, Moving least-squares particle hydrodynamics II: conservation and boundaries, Int. J. Numer. Methods Eng. 48 (10) (2000) 1503–1524.
[6] Nicholas Frontiere, Cody D. Raskin, J. Michael Owen, CRKSPH–a conservative reproducing kernel smoothed particle hydrodynamics scheme, J. Comput. Phys. 332 (2017) 160–209.
[7] Stuart C. Whitehouse, Matthew R. Bate, Smoothed particle hydrodynamics with radiative transfer in the flux-limited diffusion approximation, Mon. Not. R. Astron. Soc. 353 (4) (2004) 1078–1094.
[8] Stuart C. Whitehouse, Matthew R. Bate, Joe J. Monaghan, A faster algorithm for smoothed particle hydrodynamics with radiative transfer in the flux-limited diffusion approximation, Mon. Not. R. Astron. Soc. 364 (4) (2005) 1367–1377.
[9] Matthew R. Bate, Eric R. Keto, Combining radiative transfer and diffuse interstellar medium physics to model star formation, Mon. Not. R. Astron. Soc. 449 (3) (2015) 2643–2667.
[10] Serge Viau, Pierre Bastien, Seung-Hoon Cha, An implicit method for radiative transfer with the diffusion approximation in smooth particle hydrodynamics, Astrophys. J. 639 (1) (2006) 559.
[11] Lucio Mayer, Graeme Lufkin, Thomas Quinn, James Wadsley, Fragmentation of gravitationally unstable gaseous protoplanetary disks with radiative transfer, Astrophys. J. Lett. 661 (1) (2007) L77.
[12] Leigh Brookshaw, A method of calculating radiative heat diffusion in particle simulations, Publ. Astron. Soc. Aust. 6 (2) (1985) 207–210.
[13] Margarita Petkova, Volker Springel, An implementation of radiative transfer in the cosmological simulation code gadget, Mon. Not. R. Astron. Soc. 396 (3) (2009) 1383–1403.
[14] Gabriel Altay, Rupert AC Croft, Inti Pelupessy, Sphray: a smoothed particle hydrodynamics ray tracer for radiative transfer, Mon. Not. R. Astron. Soc. 386 (4) (2008) 1931–1946.
[15] Sergei Nayakshin, Seung-Hoon Cha, Alexander Hobbs, Dynamic Monte Carlo radiation transfer in SPH: radiation pressure force implementation, Mon. Not. R. Astron. Soc. 397 (3) (2009) 1314–1325.
[16] Christopher L. Fryer, Gabriel Rockefeller, Michael S. Warren, Snsph: a parallel three-dimensional smoothed particle radiation hydrodynamics code, Astrophys. J. 643 (1) (2006) 292.
[17] Robert B. Lowrie, A comparison of implicit time integration methods for nonlinear relaxation and diffusion, J. Comput. Phys. 196 (2) (2004) 566–590.
[18] V.A. Mousseau, D.A. Knoll, W.J. Rider, Physics-based preconditioning and the Newton–Krylov method for non-equilibrium radiation diffusion, J. Comput. Phys. 160 (2) (2000) 743–765.
[19] Jim E. Morel, Edward W. Larsen, M.K. Matzen, A synthetic acceleration scheme for radiative diffusion calculations, J. Quant. Spectrosc. Radiat. Transf. 34 (3) (1985) 243–261.
[20] Jim E. Morel, T-Y Brian Yang, James S. Warsa, Linear multifrequency-grey acceleration recast for preconditioned Krylov iterations, J. Comput. Phys. 227 (1) (2007) 244–263.
[21] Peter N. Brown, Carol S. Woodward, Preconditioning strategies for fully implicit radiation diffusion with material-energy transfer, SIAM J. Sci. Comput. 23 (2) (2001) 499–516.
[22] Hiroyuki Tetsu, Taishi Nakamoto, Comparison of implicit schemes to solve equations of radiation hydrodynamics with a flux-limited diffusion approximation: Newton–Raphson, operator splitting, and linearization, Astrophys. J. Suppl. Ser. 223 (1) (2016) 14.
[23] Paul J. Lanzkron, Donald J. Rose, James T. Wilkes, An analysis of approximate nonlinear elimination, SIAM J. Sci. Comput. 17 (2) (1996) 538–559.
[24] Thomas A. Brunner, Terry S. Haut, Paul F. Nowak, Nonlinear elimination applied to radiation diffusion, Nucl. Sci. Eng. (2020) 1–13.
[25] Hamou Sadat, On the use of a meshless method for solving radiative transfer with the discrete ordinates formulations, J. Quant. Spectrosc. Radiat. Transf. 101 (2) (2006) 263–268.
[26] L.H. Liu, J.Y. Tan, Meshless local Petrov-Galerkin approach for coupled radiative and conductive heat transfer, Int. J. Therm. Sci. 46 (7) (2007) 672–681.
[27] Manuel Kindelan, Francisco Bernal, Pedro González-Rodríguez, Miguel Moscoso, Application of the RBF meshless method to the solution of the radiative transport equation, J. Comput. Phys. 229 (5) (2010) 1897–1908.
[28] Brody Bassett, Brian Kiedrowski, Meshless local Petrov–Galerkin solution of the neutron transport equation with streamline-upwind Petrov–Galerkin stabilization, J. Comput. Phys. 377 (2019) 1–59.
[29] B. Rokrok, H. Minuchehr, A. Zolfaghari, Element-free Galerkin modeling of neutron diffusion equation in x–y geometry, Ann. Nucl. Energy 43 (2012) 39–48.
[30] Tayfun Tanbay, Bilge Ozgener, Numerical solution of the multigroup neutron diffusion equation by the meshless RBF collocation method, Math. Comput. Appl. 18 (3) (2013) 399–407.
[31] Charles K. Birdsall, Particle-in-cell charged-particle simulations, plus Monte Carlo collisions with neutral atoms PIC-MCC, IEEE Trans. Plasma Sci. 19 (2) (1991) 65–85.

[32] Robert D. Falgout, Ulrike Meier Yang, Hypre: a library of high performance preconditioners, in: International Conference on Computational Science, Springer, 2002, pp. 632–641.
[33] C.D. Levermore, Relating eddington factors to flux limiters, J. Quant. Spectrosc. Radiat. Transf. 31 (2) (1984) 149–160.
[34] J.E. Morel, Diffusion-limit asymptotics of the transport equation, the P1/3 equations, and two flux-limited diffusion theories, J. Quant. Spectrosc. Radiat. Transf. 65 (5) (2000) 769–778.
[35] Dimitri Mihalas, Barbara Weibel Mihalas, Foundations of Radiation Hydrodynamics, Courier Corporation, 2013.
[36] J.A. Fleck Jr, J.D. Cummings Jr., An implicit Monte Carlo scheme for calculating time and frequency dependent nonlinear radiation transport, J. Comput. Phys. 8 (3) (1971) 313–342.
[37] Holger Wendland, Piecewise polynomial, positive definite and compactly supported radial functions of minimal degree, Adv. Comput. Math. 4 (1) (1995) 389–396.
[38] J.I. Read, T. Hayfield, O. Agertz, Resolving mixing in smoothed particle hydrodynamics, Mon. Not. R. Astron. Soc. 405 (3) (jul 2010) 1513–1530.
[39] Walter Dehnen, Hossam Aly, Improving convergence in smoothed particle hydrodynamics simulations without pairing instability, Mon. Not. R. Astron. Soc. 425 (2) (sep 2012) 1068–1082.
[40] J. Michael Owen, ASPH modeling of material damage and failure, in: Proceedings of the 5th International SPHERIC Workshop, Manchester, UK, Jan 2010, pp. 297–304.
[41] William J. Rider, Dana A. Knoll, Time step size selection for radiation diffusion calculations, J. Comput. Phys. 152 (2) (1999) 790–795.
[42] Ernst Hairer, Gerhard Wanner, Stiff differential equations solved by Radau methods, J. Comput. Appl. Math. 111 (1–2) (1999) 93–111.
[43] Bingjing Su, Gordon L. Olson, An analytical benchmark for non-equilibrium radiative transfer in an isotropically scattering medium, Ann. Nucl. Energy 24 (13) (1997) 1035–1055.
[44] Wing Kam Liu, Sukky Jun, Yi Fei Zhang, Reproducing kernel particle methods, Int. J. Numer. Methods Fluids 20 (8–9) (1995) 1081–1106.